PROCEEDINGS OF SCIENCE

Non-thermal emission from local young massive star clusters and detection prospects with current and next generation instruments

S. Celli,[a,b,*] **A. Mitchell,**[c] **G. Morlino**[d] **and S. Menchiari**[e]

[a] *Sapienza Università di Roma, Piazzale Aldo Moro 5, 00185, Rome, Italy*

[b] *Istituto Nazionale di Fisica Nucleare, Sezione di Roma, Piazzale Aldo Moro 5, 00185, Rome, Italy*

[c] *Friedrich-Alexander-Universität Erlangen-Nürnberg, Erlangen Centre for Astroparticle Physics, Nikolaus-Fiebiger-Str. 2, 91058 Erlangen, Germany*

[d] *Istituto Nazionale di Astrofisica, Osservatorio Astrofisico di Arcetri, L.go E. Fermi 5, Firenze, Italy*

[e] *Instituto de Astrofisica de Andalucia, CSIC, 18080 Granada, Spain*

E-mail: silvia.celli@roma1.infn.it

Young and massive star clusters have been proposed as potential sources of cosmic rays reaching PeV energies, offering a complementary perspective to the supernova remnant scenario. The collective action of stellar winds in a compact cluster creates a strong wind termination shock, which may accelerate particles efficiently over million-year timescales. Supernova remnants within the cluster cores contribute an additional, eventually dominant, energy source. The subsequent hadronic interactions of these accelerated particles produce gamma rays and neutrinos. Using a model that accounts for both wind termination shock and supernova remnant contributions, we calculate the expected flux of secondary particles from the local star clusters identified by the Gaia satellite. We assess their detectability with current and next-generation observatories, including CTAO, LHAASO, and KM3NeT, employing detailed sensitivity curves for extended sources.

39th International Cosmic Ray Conference (ICRC2025)
15–24 July 2025
Geneva, Switzerland

ICRC 2025
The Astroparticle Physics Conference
Geneva July 15-24, 2025

*Speaker

PoS(ICRC2025)598

1. Introduction

Young and massive star clusters have recently been identified as promising candidates for the production of cosmic rays (CRs) in the PeV range [1, 2], challenging the conventional view that attributes this role solely to supernova remnants (SNRs). Observational evidence supports this hypothesis: several star clusters, including Westerlund 1, Westerlund 2, and the Cygnus OB2 association, have been detected in very-high-energy gamma rays. Notably, Cygnus OB2 has been observed by the Large High Altitude Air Shower Observatory (LHAASO) to be surrounded by an extended bubble containing 66 photon-like events above 400 TeV, including 8 with energies exceeding 1 PeV [3]. These findings suggest a contribution by star clusters to the Galactic CR flux.

However, the precise location and mechanisms responsible for efficient particle acceleration in these environments remain uncertain. Potential acceleration sites include collective wind termination shocks (WTS) generated by massive stellar winds [4], SNR shocks forming later within cluster cores [5], and even regions of colliding stellar winds [6]. The efficiency and relative contributions of these mechanisms depend on various factors, e.g. the cluster's age and the level of magnetic turbulence. The former is critical as it determines the presence or absence of SNRs: specifically, clusters aged between 3 and 30 Myr are expected to host supernova (SN) events, which rapidly surpass stellar winds in mechanical power. This age range is based on the evolution of solar-metallicity stars, with the most massive stars ($\sim 150 M_{\odot}$) exploding after 2-3 Myr, and the lowest-mass SN progenitors ($8 M_{\odot}$) requiring around 30 Myr [7]. Moreover, the development of magnetic turbulence is among the main sources of uncertainty in modeling particle acceleration and transport: depending on the diffusion regime (e.g., Bohm, Kraichnan, Kolmogorov), the emerging spectral energy distribution and the achievable particle maximum energy can vary significantly.

Our study focuses on Milky Way star clusters younger than 30 Myr, aiming to assess whether these systems can accelerate particles to PeV energies and to predict the associated radiation signatures. Modeling the hadronic emission from such clusters is complex, requiring knowledge of stellar populations in clusters, wind physics at different evolutionary stages, dynamical evolution of these systems (including winds, SNRs, and magnetic turbulence), particle acceleration processes, and the distribution of target gas. In the following sections, we describe our methodology: Sec. 2 presents the cluster sample derived from Gaia data and an estimation of their wind luminosities; Sec. 3 outlines the acceleration model, incorporating both the WTS and SNRs; Sec. 4 details the calculation of secondary emission from hadronic interactions; and Sec. 5 evaluates the prospects for detecting this emission with next-generation instruments. Lastly, we conclude in Sec. 6.

2. The cluster sample

Our study adopts the second data release (DR2) from the Gaia space observatory as the reference dataset for identifying young star clusters near the Solar System. The full catalog contains 1857 clusters [8]. To focus on clusters likely to host SNRs, we apply a selection criterion that limits the sample to objects younger than 30 Myr. A further selection is based on key stellar parameters such as effective temperature and extinction, required to evaluate the cluster mass and wind luminosity.

After filtering, we obtain a sample of 387 clusters. More detailed information on the selection process and calculations can be found in [9]. For these interesting clusters, we estimate a lower

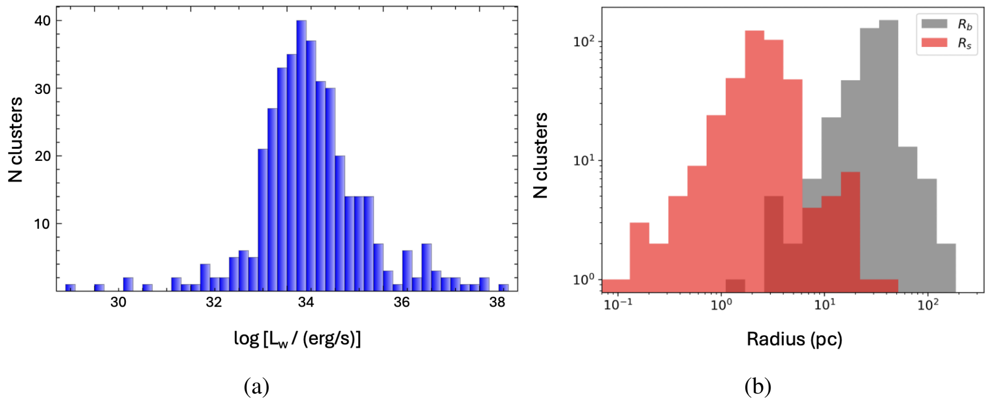

Figure 1: (a) Wind luminosity of selected young clusters from Gaia DR2 release [9]. (b) Bubble and WTS radii of the same cluster sample [11].

limit of both cluster mass and wind luminosity (L_w). The latter, shown in Fig. 1(a), is essential for scaling the CR production efficiency in the various acceleration models discussed next.

3. The particle acceleration model: WTS and SNRs

Massive stars lose a significant fraction of their mass via stellar winds during their evolution. Stellar associations can form a collective wind, that is launched together with a forward and a reverse shock. The former is a mild shock compressing the interstellar medium (ISM), delimiting the bubble at radius R_b, with a modest efficiency in particle acceleration [4]. The latter, also known as wind termination shock, is sustained by the ram pressure of the wind. A star cluster is compact if its WTS position R_s is located beyond the cluster radius R_c: for compact clusters, the WTS is strong with a typical Mach number of 5-10 [10], hence, in principle, effective in accelerating particles. The positions of these two shocks depend on the wind luminosity, cluster age, surrounding ISM density n_0 and on the radiative cooling efficiency, which impact the energy transferred to the mechanical component of the wind itself. The ISM density can be inferred from a relation between the cluster mass and the mass of its parent Giant Molecular Cloud (GMC), assuming 10% star formation efficiency and GMC mass-radius relations as in [14] and [15]. On the other hand, the cooling fraction depends on many parameters, including cluster age and n_0: it is here fixed to 30% following numerical simulations by [12]. For the selected cluster sample, the resulting R_s and R_b distributions are shown in Fig. 1(b), assuming the adiabatic wind blown bubble model by [17].

Particle transport within the bubble is governed by the interplay between diffusion and advection. The WTS-accelerated spectrum can be obtained by iteratively solving the stationary transport equation in spherical symmetry, including diffusion, advection, injection, and adiabatic losses [4]. Limiting our analysis to protons, the result is a power-law spectral energy distribution, whose slope (here set equal to -4) depends on the compression ratio, modified by a high-energy cut-off, which is rather determined by upstream particle confinement and escape from the bubble. Specifically, the shape of the cut-off depends on the diffusion regime: for a fixed maximum energy, Bohm diffusion would produce a sharper cut-off. Far from the WTS, the radial particle profile is flat in the advection-dominated regime and decreases radially under diffusion-dominated conditions [13]. We assume a standard 10% efficiency for converting the wind kinetic energy into non-thermal particles and magnetic turbulence.

Supernova explosions provide an additional source of particle acceleration, eventually dominant after a few million years. Due to their short active phases (~ 0.05 Myr), SNRs act as transient phenomena across the cluster evolution, introducing non-stationary effects in the particle transport and potentially generating multiple reflected shocks, leading to a highly non-uniform environment within the bubble itself. Modeling such dynamics requires detailed magneto-hydrodynamic simulations, which are beyond the scope of this work. We instead proceed by considering the number of SNe as evaluated in [9] and adopting the following simplifying assumptions:

- all SNe release 10^{51} erg of kinetic energy;
- the SNR mechanical power contributes to the cluster luminosity, enlarging the bubble size with respect purely wind driven case;
- the SNR ejecta contribute to the bubble mass, thus enhancing its density, as described next;
- the maximum particle energy achieved by SNRs is determined by a time-limited condition, i.e. by equating the acceleration time to the Sedov time in the ambient magnetic field (~ 10μG) provided by the WTS turbulence as well as that excited by the CR driven turbulence (see [11] for further insights). The latter effect is also expected to lead to steeper spectral slopes than -4, here taken to be -4.3.
- because the SNR maximum energy decreases during the Sedov stage, particle acceleration is expected to be dominated by the early (ejecta-dominated) phase of SNRs;
- since the SNR radius at Sedov time is similar to the WTS size, particles are directly injected at the WTS and propagated as in the WTS scenario [4];
- only SNe occurring within the last escape time will contribute to the actual CR distribution inside the bubble.

As a result, at a fixed particle momentum, the ratio between the CR density produced by SNRs and WTS is found to scale with the ratio between the energetics of all SNe occurred in the last advection time and the mechanical energy provided by the wind in the same time [11]. The SNR-accelerated spectrum also follows a power-law, with a different cut-off energy than that produced at the WTS. Fig. 2 compares the maximum energy for WTS and SNR acceleration, where each dot represents each of the selected cluster by the Gaia DR2 sample, and the different colors refer to different possible diffusion regimes. On average, the maximum energy by SNRs exceeds that from the WTS, with a positive correlation between these two quantities linked to the enhanced magnetic turbulence from powerful stellar winds. Interestingly, several clusters exhibits maximum energies in the PeV domain, which are therefore interesting targets for PeVatron searches.

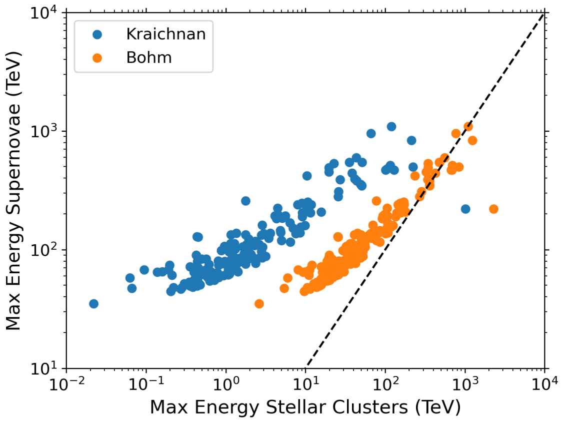

Figure 2: Predicted maximum proton energy from acceleration at the WTS (x-axis) compared to that due to SNRs (y-axis) for star clusters in our sample, assuming Kraichnan or Bohm diffusion in the bubble. The dashed line shows $E_{\rm max}^{\rm SNR} = E_{\rm max}^{\rm WTS}$.

4. Production of gamma rays and neutrinos via hadro-nuclear collisions

Hadronic interactions between accelerated protons and ambient gas result in the production of energetic photons and neutrinos, mostly from the decay of neutral and charged pions respectively. We follow the procedure in [16] for the computation of the gamma-ray and neutrino emission for each cluster. A critical component in this computation is the radial profile of the target gas mass density within the bubble, whose description follows [17]. Specifically, inside the cluster core radius $R_{\rm c}$ we assume a constant number density, whose value is fixed by a continuity condition with the cold wind profile:

$$n_{\rm w}(r) = \frac{\dot{M}_{\rm c}}{4\pi r^2 v_{\rm w}\, m_p} \qquad R_{\rm c} \le r < R_{\rm s}$$

m_p being the proton mass, $\dot{M}_{\rm c}$ the cluster mass-loss rate, and v_w the wind velocity, both taken from [9]. In the hot wind region, namely between $R_{\rm s}$ and the contact discontinuity located at $r = R_{\rm cd}$, the density n_b is again taken to be constant, this time determined by:

- the wind-injected mass
$$M_{\rm w}(t) = \dot{M}_{\rm c}\, t - \frac{\dot{M}_{\rm c}(R_{\rm s} - R_{\rm c})}{v_{\rm w}}$$
where the second term represents the mass going into the cold wind region;
- the mass evaporated from the outer shell $M_{\rm sh}$, whose loss-rate is [17]:
$$\dot{M}_{\rm sh}(t) = 2\times 10^{-4} \left(\frac{L_{\rm w}}{10^{37}\,{\rm erg/s}}\right)^{\frac{27}{35}} \left(\frac{n_0}{10\,{\rm cm}^{-3}}\right)^{-\frac{2}{35}} \left(\frac{t}{1\,{\rm Myr}}\right)^{\frac{6}{35}} \; M_\odot\,{\rm yr}^{-1}$$
such that the total mass present within the bubble depends on the cluster wind luminosity. Given its weak dependence on time, we treat the mass evaporation rate of the shell as constant and compute the amount of evaporated mass from the shell as $M_{\rm sh} = \dot{M}_{\rm sh}(t)t$.

- the mass coming from the ejecta $M_{\rm ej}$ of all SN explosions occurred during the cluster lifetime $N_{\rm sn}(t)$.

As such, the total mass in the bubble reads as

$$M_{\rm b}(t) = (\dot{M}_{\rm sh} + \dot{M}_{\rm w})\, t - \frac{\dot{M}_{\rm w}(R_{\rm s} - R_{\rm c})}{v_{\rm w}} + N_{\rm sn}(t) M_{\rm ej}$$

and the corresponding average density as

$$n_{\rm b} = \frac{M_{\rm b}}{\frac{4}{3}\pi \left(R_{\rm cd}^3 - R_{\rm s}^3\right) m_{\rm p}}$$

Finally, the shell density is derived from the compressed ISM density, corresponding to the entire amount of swept-up mass depleted by the evaporated shell mass, as:

$$n_{\rm sh} = \frac{n_0}{1 - R_{\rm cd}^3/R_{\rm b}^3} - \frac{\dot{M}_{\rm sh} t}{m_{\rm p} V_{\rm sh}}$$

where $V_{\rm sh}$ is the volume of the shell embedded between $R_{\rm cd} \simeq 0.95 R_{\rm b}$ and $R_{\rm b}$.

While the reference model for the current study [17] assumes a spherical shell of swept up material, numerical simulations [18] show that the shell usually fragments in a complex fractal structure of filaments and clumps as a consequence of hydrodynamical instabilities. This increases the effective target gas density inside the bubble, enhancing the flux of secondary particles with a harder spectrum: indeed, due to energy-dependent diffusion, the CR spectrum softens toward the bubble boundary [4]. Such an effect is here accounted uniquely for the purpose of estimating the uncertainties in our final calculation, therefore in the following we simply set either no fragmentation or a 10% fraction of the shell material fragmenting into dense clumps that uniformly fill the bubble.

5. Detection prospects with current and next-generation instruments

To calculate the expected hadronic gamma-ray and neutrino emission from the wind-blown bubbles of the sample, also including different sources of uncertainty, we define two limiting cases:

- *minimal* model: particles accelerated at the WTS only, with wind luminosity as in [9], and no shell fragmentation;
- *maximal* model: with respect to the above scenario, we here set a 3 times higher wind luminosity, further including SNRs, with shell fragmentation.

We further define a *baseline* scenario which is represented by the minimal model with particle transport following Kraichnan diffusion. Finally, we also vary the ISM density using two different GMC mass-radius relations, with [14] for the minimal and baseline scenarios, and [15] for the maximal one. Cluster bubbles typically span 10-100 pc (see Fig. 1(b)), resulting in degree-scale angular sizes. Therefore, detection prospects are more realistically evaluated through the comparison with instrument sensitivities for extended sources, especially for high-resolution pointing

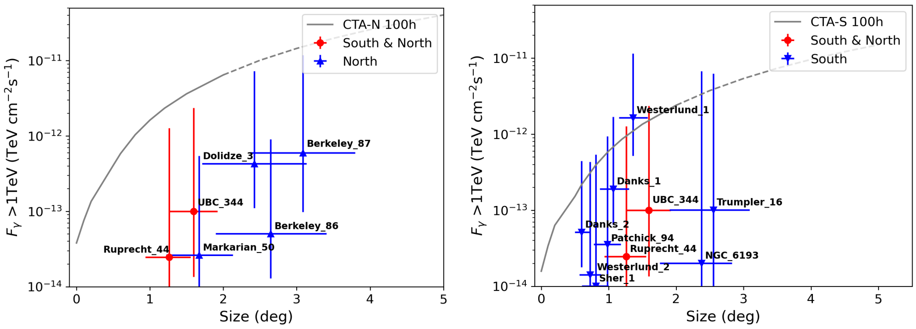

Figure 3: Integral gamma-ray flux above 1 TeV from clusters as a function of the bubble size. The CTAO sensitivity for 100 hr observation is shown for comparison [19]. *Left:* CTA-North. *Right:* CTA-South. The uncertainties show the minimal and maximal predictions from the Kraichnan diffusion model for each cluster.

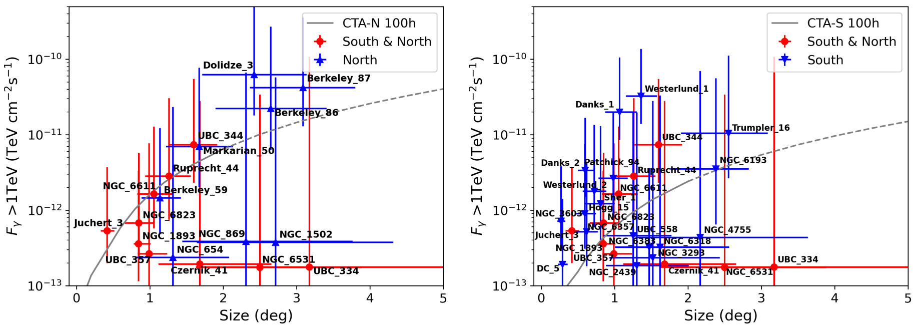

Figure 4: Same as previous figure, with minimal and maximal predictions from the Bohm diffusion model.

instruments as the Cherenkov Telescope Array Observatory (CTAO) [19]. Figs. 3 and 4 show the predicted integral gamma-ray fluxes from the cluster bubbles for Kraichnan and Bohm diffusion respectively, as compared to the expected 100 hour sensitivity of the Northern and Southern arrays at the corresponding angular bubble size. The Bohm case results the most promising in terms of detection prospects, due to the enhanced confinement properties of this diffusion domain. The error bars reflect the range between minimal and maximal model predictions, affecting both the absolute flux as well as the expected size of the emitting bubble. Despite many predicted fluxes exceeding the point-like sensitivity of these detectors, they often fall below the degraded sensitivity thresholds for extended sources, suggesting longer observation times for a detection. In any case, observations by next-generation instrument will be of paramount importance to test this model. The comparison of our gamma-ray predictions with catalogued LHAASO sources is provided in [11].

The detection of accompanying neutrinos will be analogously challenging. Fig. 5 shows predicted muon neutrino spectra, this flavor channel having the best performance in terms of angular resolution capabilities, especially in water-based Cherenkov telescopes as KM3NeT, whose 10 yr sensitivity is shown for comparison [20]. Among the investigated cluster sample, Westerlund 1 is expected to yield the strongest signal, nearly reaching detectability in the maximal scenario. Stacking analyses of the entire cluster sample might provide more promising results.

PoS(ICRC2025)598

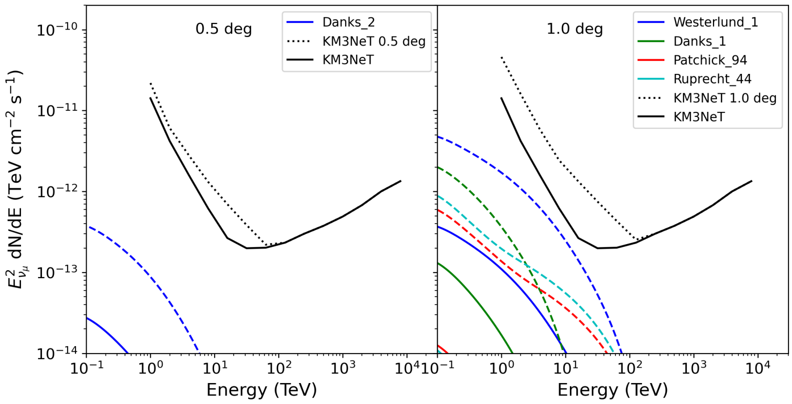

Figure 5: Predicted single-flavor muon neutrino spectral energy distributions from the wind-blown bubbles, with angular size in the baseline scenario comparable to (i.e. within 0.25° of) 0.5° (left) and 1.0° (right). Each source is shown with two colored lines representing the minimal (solid) and maximal (dashed) models for the case of Kraichnan diffusion. Sensitivity curves for KM3NeT in 10 year exposure are also shown for reference [20]: solid line for the point-like case, dashed for the extended one with 1° radius.

6. Conclusions

The predicted gamma-ray and neutrino fluxes from hadronic collisions in WTS and SNR environments of the Gaia DR2 star cluster sample are within the reach of next-generation observatories. However, due to their large angular sizes, the detection of star clusters is especially difficult for pointing instruments like CTAO. Nonetheless, their cumulative contribution to diffuse Galactic emissions might be non-negligible. This effect is being considered in [21] in the context of the same model, via the simulation of a synthetic cluster sample along the entire Milky Way.

References

[1] F. Aharonian et al., Nature Astronomy **3** (2019) 561;
[2] T. Vieu et al., MNRAS **519** (2023) 136V;
[3] LHAASO Collaboration, Science Bulletin **69** (2024) 449;
[4] G. Morlino, P. Blasi, E. Peretti & P. Cristofari, MNRAS **504** (2021) 6069;
[5] T. Vieu et al., MNRAS **512** (2022) 1275;
[6] A. Bykov et al., Advances in Space Research, **64** (2019) 12;
[7] A. Buzzoni, ApJ **123** (2002) 1188;
[8] Gaia Collaboration, A&A **640** (2020) A1;
[9] S. Celli et al., A&A **686** (2024) A118;
[10] S. Gupta et al., MNRAS **493** (2020) 3159;
[11] A. Mitchell et al., arXiv:2403.16650;
[12] N. Yadav et al. MNRAS **465** (2017) 1720;
[13] S. Menchiari et al., A&A 686A (2024) 242M;
[14] Y. Sun et al., ApJS **275** (2024) 35;
[15] B. Q. Chen et al., MNRAS **493** (2020) 351;
[16] S. R. Kelner et al., Phys. Rev. D **74** (2006) 034018;
[17] R. Weaver et al., ApJ **218** (1977) 377;
[18] L. Lancaster et al., ApJ **914** (2021) 89;
[19] S. Celli & G. Peron, A&A **689** (2024) A258;
[20] L. Ambrogi et al., Astropart. Phys. **100** (2018) 69;
[21] S. Menchiari, S. Celli et al., PoS (ICRC2025) 1010.